Supplemental material for : "Fracture initiation in silicate glasses via a universal shear localization mechanism"

Matthieu Bourguignon,[1] Gustavo Alberto Rosales-Sosa,[2] Yoshinari Kato,[2] Bruno Bresson,[1] Hikaru Ikeda,[2] Shingo Nakane,[2] Gergely Molnár,[3] Hiroki Yamazaki,[2] and Etienne Barthel[1]

[1]*Soft Matter Sciences and Engineering, ESPCI Paris, PSL University, CNRS, Sorbonne University, 75005 Paris, France.*

[2]*Nippon Electric Glass, 7-1, Seiran 2-Chome, Otsu, 520-8639, Shiga, Japan.*

[3]*CNRS, INSA Lyon, LaMCoS, UMR5259, 69621 Villeurbanne, France*

(Dated: March 28, 2026)

S I. EXPERIMENTAL PROCEDURES

A. Sample preparation

Batches were mixed to yield 500 g of glass using industrial grade raw materials: silicon oxide SiO_2 (99.9%), boric acid H_3BO_3 (56.8 wt%), aluminum oxide Al_2O_3 (99.9 wt%), calcium carbonate $CaCO_3$ (55.5 wt%) and magnesium oxide MgO (99.3 wt%). After batches were prepared, small amounts (0.1 wt% of the total batch) of fining agent SnO_2 were added to allow the removal of gas bubbles from the melt. For each batch, weighted raw materials were first melted in a 300 cc Pt-Rh crucible for 15h at a temperature of 1500 °C in an electric furnace and stirred one first time using a platinum rod to improve the homogeneity of the melt. After letting melt overnight (around 15h), the batch materials were stirred periodically and melted again at T_m + 30 °C for 3h. An approximation of their glass transition temperature T_g was determined by using the Facstage® and Interglad® softwares, based on the viscosity calculation of each melt. Melted glasses were poured onto a carbon plate and placed in an electric furnace to cool slowly. They were annealed at T_g + 30 °C for 1h and then cooled at 3 °C/min up to room temperature to reduce residual thermal stresses. All obtained glasses were transparent except the composition $15MgO \cdot 15Al_2O_3 \cdot 25B_2O_3 \cdot 45SiO_2$ which showed a "bluish" transparent color after annealing probably due to phase separation. Each annealed glass was then cut and processed into several different samples. The glass transition temperature was precisely determined by a dilatometer (see next section). Finally, samples of the glasses were heated up in an annealer at 5 °C/min up to T_g + 30 °C, held for 30 min, cooled at 3 °C/min down to T_g - 150 °C and then cooled at 5°C/min down to room temperature to reduce residual mechanical stresses from post-processing.

Table S1. Single alkaline earth aluminoborosilicate glass compositions

Glass	SiO_2 (mol %)	B_2O_3 (mol %)	Al_2O_3 (mol %)	CaO (mol %)	MgO (mol %)
CAS1	70	-	15	15	-
CABS2	65	5	15	15	-
CABS3	55	15	15	15	-
CABS4	45	25	15	15	-
MAS1	70	-	15	-	15
MABS2	65	5	15	-	15
MABS3	55	15	15	-	15
MABS4	45	25	15	-	15

Table S2. Dual alkaline earth aluminoborosilicate glass compositions.

Glass	SiO_2 (mol %)	B_2O_3 (mol %)	Al_2O_3 (mol %)	CaO (mol %)	MgO (mol %)
CMABS1	65	5	15	12.5	2.5
CMABS2	65	5	15	10	5
CMABS3	65	5	15	7.5	7.5
CMABS4	65	5	15	5	10
CMABS5	65	5	15	2.5	12.5
CMABS6	55	15	15	12.5	2.5
CMABS7	55	15	15	10	5
CMABS8	55	15	15	7.5	7.5
CMABS9	55	15	15	5	10
CMABS10	55	15	15	2.5	12.5

Measurement of glass properties

The glass transition temperature T_g and coefficient of thermal expansion CTE were estimated with thermomechanical analysis (TMA) by using a Bruker AXS TD5000SA machine (differential dilatometer) under He gas flow. The maximum temperature that can be reached is around 900°C and a heating rate of 3°C/min was applied. Those measurements have been performed by a technician from NEG company.

Density was determined using Archimedes' method (water displacement) with an uncertainty of ± 0.0002 g/cm^3. Young's modulus (E) and shear modulus (G) were measured by resonance method using the ASTM standard issued under the fixed designation E1875-08, with 40 × 20 × 2 mm^3 samples. A Japan Techno-Plus JE-RT3 with Young's modulus (JR-RT) and Shear Modulus (JG) modules were used to estimate these two elastic moduli. Each sample was first gold coated for 2 min. The frequency at which the measured intensity is highest is defined as the resonance frequency f. From this value, we can calculate Young's modulus E and shear modulus G from the sample dimensions with the following equations:

$$E = 0.9465 \cdot \frac{Mf^2}{w} \cdot \left(\frac{L}{t}\right)^3 \cdot \left(1 + 6.59\left(\frac{t}{L}\right)^2\right) \tag{S1}$$

$$G = 3.933 \cdot \frac{MLf^2}{wt} \cdot \left(\frac{s + 1/s}{4s - 2.52s^2 + 0.21s^6}\right) \tag{S2}$$

where L is the length of the sample, t is the thickness, w is the width, M is the weight, and $s = t/w$. The bulk modulus (K) and the Poisson ratio (ν) were then calculated using the standard relations:

$$K = \frac{EG}{(9G - 3E)} \tag{S3}$$

$$\nu = \frac{E}{2G} - 1 \tag{S4}$$

To determine Vickers hardness, 30 indents were made at 100 gf and a dwelling time of 15 s with a microhardness tester (MXT50, Matsuzawa Seiki Corp., Japan). Diagonals for each indent were measured and the Vickers hardness (H_V) values were then calculated using the following equation:

$$H_V = \frac{2\sin\left(\frac{\theta}{2}\right) \cdot F}{D^2} = \frac{1.8544 \cdot F}{D^2} \tag{S5}$$

where F is the applied load, θ is the 136° angle between opposite faces of the Vickers tip, and D is the diagonal length of the indent. The hardness unit is HV (or kgf/mm). To convert HV to GPa, we have to multiply by 0.009807.

Plastic flow characterization

Cross-sections of 500 gf and 1 kgf Vickers indents were prepared by using Peter's method [1] which has been used later by Hagan [2] and more recently by Gross [3]. This technique involves indenting across a pre-existing crack introduced into a $25 \times 5 \times 1$ mm^3 glass specimen by performing a line of dozen indentations at 1 kgf. The crack is slowly propagated with a 3-point bending setup until it reaches 1 mm in length from each side of the indents line. When the load is released, a part of the crack becomes invisible. Indentations at several loads were then made along the crack at different positions. The distance between two indents must be at least 100 µm to prevent the stress field of the previous indent from affecting the indentation pattern of the next one. The two faces of the glass specimen are finally separated by fully propagating the pre-existing crack with the same 3-point bending setup.

Laser Scanning Microscope (LSM)

The indentation cross-sections from both sides have been observed at the Nippon Electric Glass Co.,Ltd. with a VK-X250K/X260K Laser Scanning Microscope from KEYENCE company. The observation was performed with the highest magnification (X28k) and a single scan mode was used. Samples were fixed vertically on the holder with double-face tape to observe their edges where the plastically deformed region of the indentation cross-section is located.

Roughness and spacing measurements

The roughness of the plastically deformed region under indents was determined by using the multi-line roughness measurement from the MultiFileAnalyzer software (VK-H1XME, KEYENCE). This function sets multiple measurement lines parallel to an initial line given by the user and calculates the roughness Ra of each line with

$$Ra = \frac{1}{l_r} \int_0^{l_r} |Z(x) - \overline{Z}| \, dx \tag{S6}$$

Similarly, the characteristic length between roughness features was measured from

$$Rsm = \frac{1}{m} \sum_{i=1}^{m} Xsi \tag{S7}$$

Concerning the Rsm value, Xsi is the length of a single profile element. The peaks (valley) will be treated as noise and considered a part of the preceding valley (peak) if the height (depth) is less than 10% of the maximum height or the length is less than 1% of the segment length.

Scanning Electron Microscopy (SEM)

The indentation cross-sections on soda-lime silicate glass were observed in ESPCI with a Quattro Environmental Scanning Electron Microscope (ESEM - ThermoFisher®). Observations were conducted at room temperature and in a low vacuum mode under a 100 Pa atmosphere. This mode allows the observation of the sample without gold coating.

B. Mechanical and thermal characterization

Results of ρ, T_g, E, G, K, ν, H_v and σ_y are shown in **Table S3** and **S4**. For all glasses (single or mixed alkaline earth network modifiers compositions), density decreases as B_2O_3 or MgO increases. Concerning the thermal characterization, T_g decreases with the addition of B_2O_3 (Fig. S1). Indeed, substituting a four-coordinated silica with a three-coordinated boron tends to gradually depolymerize the network and decrease the glass transition temperature. For a composition with 5% B_2O_3, T_g slightly decreases as MgO increases but it remains unchanged with 15% B_2O_3. The values of E, G, K, and H_v decrease with increasing B_2O_3 but increase (slightly concerning elastic moduli) with increasing MgO. This evolution of E is consistent with the predictions of the Makishima-MacKenzie model [4] assuming a 100% B(III) speciation, as expected for these compositions (Fig. S2).

On the other hand, the Poisson's ratio experiences minimal variation with the addition of boron, and remains generally unaffected by the substitution of calcium for magnesium.

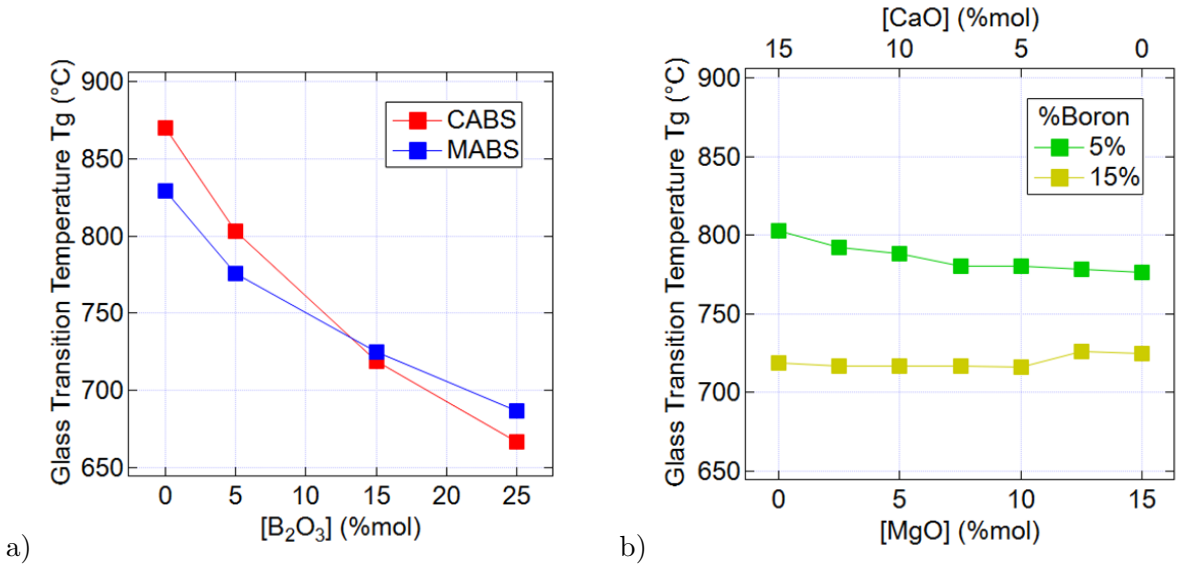

Figure S1. Glass transition temperature T_g of (a) single alkaline earth ABS glasses as a function of B_2O_3 content and (b) mixed alkaline earth ABS glasses as a function of MgO/CaO content. Error bars are smaller than the markers' size.

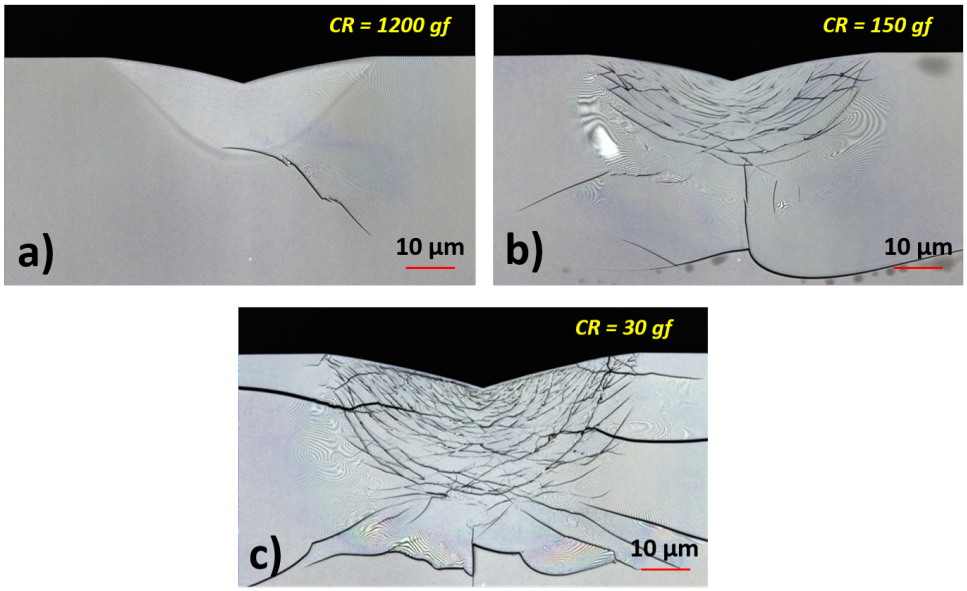

Figure S3. Cross-sections through 1 kgf Vickers indents in (a) aluminoborosilicate, (b) soda-lime silicate and (c) lead silicate.

Their crack resistance values for the three commercial glasses LS, SLS and ABS studied in [5] are taken from the same paper, but they have not been measured again for this work.

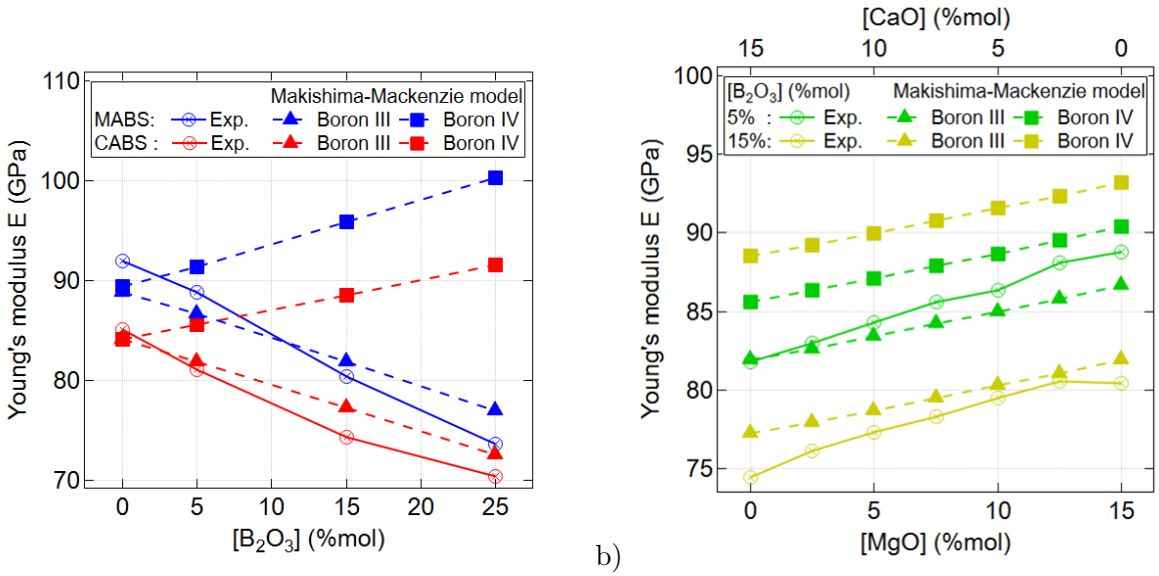

Figure S2. Comparison of Young's modulus obtained experimentally with Makishima-Mackenzie model [4] depending on the boron coordination for (a) single alkaline earth ABS glasses and (b) mixed alkaline earth ABS glasses.

The ABS glass (**Fig. S3 (a)**) doesn't show any shear localization within the deformation zone. However, this glass is more sensitive to cracking than a 25% B_2O_3 glass composition (CABS4 for instance) whose deformation zone doesn't show any shear pattern as well. On the other hand, soda-lime silicate glass (**Fig. S3 (b)**) and lead silicate glass(**Fig. S3 (c)**) exhibit significant shear faulting over all their deformation zones and also have a very high cracking resistance.

S II. MOLECULAR DYNAMICS (STATICS) SIMULATION PROCEDURE

A. Potential function

We adopted the SHIK potential [6] [7] developed by Kob and co-workers as the force field model for molecular dynamics simulations. In this potential, the long-range Coulombic interactions are evaluated by the Wolf summation method [8], while the short-range interactions employ the Buckingham functional form [9].

$$U_{ij}(r_{ij}) = A_{ij}\exp(-B_{ij}r_{ij}) - \frac{C_{ij}}{r_{ij}^6} + \frac{D_{ij}}{r_{ij}^{24}} + U_{ij}^W(r_{ij}) \tag{S8}$$

Where,

Table S3. Density (ρ), Glass transition temperature (T_g), Young's modulus (E), Shear modulus (G), Bulk modulus (K), Poisson's ratio (ν), Vickers hardness (H_V), Yield stress (σ_y), Crack resistance (CR) and Recovery indentation depth (RID) of single alkaline earth network modifier ABS glasses.

Glass	ρ (g/cm^3)	T_g (°C)	E (GPa)	G (GPa)	K (GPa)	ν	H_V (GPa)	σ_y (GPa)	CR (N)	RID (%)
CAS1	2.52	870	85.1	35.1	49.6	0.21	7.1	3.5	3	30
CABS2	2.49	803	81.0	33.3	47.7	0.22	6.6	3.4	9	33
CABS3	2.45	719	74.4	30.1	46.9	0.24	6.1	3.1	23	29
CABS4	2.42	667	70.4	28.1	47.0	0.25	5.8	2.7	25	26
MAS1	2.48	829	92.0	37.8	54.2	0.22	7.8	3.8	27	30
MABS2	2.46	776	88.8	36.4	52.8	0.22	7.7	3.7	28	26
MABS3	2.41	725	80.4	32.7	49.5	0.23	7.0	3.3	29	25
MABS4	2.37	687	73.6	29.8	46.3	0.24	6.5	3.1	33	27

Experimental uncertainties are as follows: ρ: ±0.01 g/cm^3; T_g: ±2 °C; E, K and G: ±0.1 GPa; ν: ±0.01; H_v: ±0.1 GPa; σ_y: ±0.1 GPa; CR: ±1 N; RID: ±1 %

$$U_{ij}^{W}(r_{ij}) = z_i z_j \left[\frac{1}{r_{ij}} - \frac{1}{r_{cut}^{W}} + \frac{(r_{ij} - r_{cut}^{W})}{(r_{cut}^{W})^2} \right] \tag{S9}$$

The short-range interactions were truncated at 8 Å, and the long-range Coulombic interactions were truncated at $r_{cut}^{W} = 10$ Å. To maintain continuity of both the potential and forces, the following smoothing function $G_{ij}(r_{ij})$ was multiplied:

$$G_{ij}(r_{ij}) = \exp\left(- \frac{\gamma^2}{(r_{ij} - r_{cut})^2} \right) \tag{S10}$$

where the width of the smoothing function γ is 0.3 Å, and r_{cut} is the short-range cutoff distance. The charges z of Si, Al, and Ca are fixed, while the charge of O adopts a value that varies depending on the glass composition. In the reference [6], $\gamma = 0.2$ Å was adopted for smoothing the potential function, but in this study, we used $\gamma = 0.3$ Å. This is to suppress numerical oscillations in the stress-strain curve during unloading in deformation simulations

Table S4. Density (ρ), Glass transition temperature (T_g), Young's modulus (E), Shear modulus (G), Bulk modulus (K), Poisson's ratio (ν), Vickers hardness (H_V), Yield stress (σ_y), Crack resistance (CR) and Recovery indentation depth (RID) of mixed alkaline earth network modifiers ABS glasses.

Glass	ρ (g/cm^3)	T_g (°C)	E (GPa)	G (GPa)	K (GPa)	ν	H_V (GPa)	σ_y (GPa)	CR (N)	RID (%)
CMABS1	2.49	792	83.0	34.0	49.4	0.22	6.8	3.5	7	31
CMABS2	2.48	788	84.3	34.5	50.1	0.22	6.9	3.6	8	29
CMABS3	2.47	780	85.6	35.1	50.7	0.22	7.2	3.6	16	30
CMABS4	2.47	780	86.3	35.4	51.2	0.22	7.3	3.7	21	28
CMABS5	2.46	778	88.1	36.1	52.4	0.22	7.6	3.7	29	28
CMABS6	2.44	717	76.1	30.9	47.6	0.23	6.2	3.2	30	29
CMABS7	2.44	717	77.3	31.4	47.8	0.23	6.3	3.2	31	29
CMABS8	2.43	717	78.3	31.8	48.5	0.23	6.4	3.2	32	26
CMABS9	2.42	716	79.5	32.3	49.3	0.23	6.7	3.3	32	27
CMABS10	2.42	716	80.5	32.7	49.9	0.23	6.9	3.3	32	27

Experimental uncertainties are as follows: ρ: ±0.01 g/cm^3; T_g: ±2 °C; E, K and G: ±0.1 GPa; ν: ±0.01; H_v: ±0.1 GPa; σ_y: ±0.1 GPa; CR: ±1 N; RID: ±1 %

and obtain a smoother response. We verified the effect of changing γ on Young's modulus and the main features of the stress-strain curve and confirmed that no significant difference occurred in the physical property values. Therefore, we judged that the adoption of γ = 0.3 Å contributes to improving simulation stability without compromising physical validity. Table B1 shows a list of the interaction parameters we employed.

B. Glass model generation

We prepared a rectangular model of 100×600×100 Å containing approximately 480,000 atoms with periodic boundary conditions to evaluate the shear bands generated during

Table B1. Short-range interaction parameters.

i-j	A_{ij} (eV)	B_{ij} (Å^{-1})	C_{ij} (eV·Å^6)	D_{ij} (eV·Å^{24})
Si-Si	2798.0	4.4073	0.0	3423204
Si-Ca	77366.0	5.0770	0.0	16800
Si-O	23108.0	5.0979	139.70	66
Al-Al	1799.1	3.6778	100.0	16800
Al-O	21740.0	5.3054	65.815	66
Ca-Ca	21633.0	3.2562	0.0	16800
Ca-O	146905.0	5.6094	45.073	16800
O-O	1120.5	2.8927	26.132	16800

shear deformation of glass. An initial model with randomly placed atoms was generated, and structural equilibration was performed at 3000 K for 100 ps. Subsequently, the system was quenched to 10^{-5} K at a cooling rate of 10 K/ps.These processes were controlled by the NPT ensemble. After that, structural relaxation was performed in the NVT ensemble for 100 ps, followed by relaxation in the NVE ensemble for 100 ps. Through these processes, a quenched glass model was obtained [10].

C. Glass model deformation simulation

We conducted simple shear deformation simulations of the glass under conditions without applying hydrostatic pressure to the model. The shear strain was applied by tilting the simulation box size in the xy plane. During this process, the dimensions of the simulation box were controlled at constant displacement steps to ensure that no hydrostatic pressure was applied to the model, i.e., the pressure in each axis satisfied $\sigma_{xx} = \sigma_{yy} = \sigma_{zz} = 0$. After model size control, atomic positions were relaxed by minimizing the total potential energy of the system. This deformation process was repeated until the accumulated strain reached

a specified value. The unloading process followed the same procedure.

---

[1] K. Peter, Densification and flow phenomena of glass in indentation experiments, Journal of Non-Crystalline Solids **5**, 103 (1970).

[2] J. T. Hagan, Shear deformation under pyramidal indentations in soda-lime glass, J. Mater. Sci. **15**, 1417 (1980).

[3] T. Gross, J. Wu, D. Baker, J. Price, and R. Yongsunthon, Crack-resistant glass with high shear band density, Journal of Non-Crystalline Solids **494**, 13 (2018).

[4] A. Makishima and J. Mackenzie, Direct calculation of young's modulus of glass, Journal of Non-Crystalline Solids **12**, 35 (1973).

[5] Y. Kato, H. Yamazaki, S. Yoshida, and J. Matsuoka, Effect of densification on crack initiation under vickers indentation test, Journal of Non-Crystalline Solids **356**, 1768 (2010).

[6] S. Sundararaman, L. Huang, S. Ispas, and W. Kob, New optimization scheme to obtain interaction potentials for oxide glasses, The Journal of Chemical Physics **148**, 194504 (2018).

[7] Y.-T. Shih, S. Sundararaman, S. Ispas, and L. Huang, New interaction potentials for alkaline earth silicate and borate glasses, Journal of Non-Crystalline Solids **565**, 120853 (2021).

[8] D. Wolf, P. Keblinski, S. R. Phillpot, and J. Eggebrecht, Exact method for the simulation of Coulombic systems by spherically truncated, pairwise r^{-1} summation, The Journal of Chemical Physics **110**, 8254 (1999).

[9] R. Buckingham, The classical equation of state of gaseous helium, neon and argon, Proceedings of the Royal Society of London. Series A. Mathematical and Physical Sciences **168**, 264 (1938).

[10] G. Molnár, P. Ganster, J. Török, and A. Tanguy, Sodium effect on static mechanical behavior of MD-modeled sodium silicate glasses, Journal of Non-Crystalline Solids **440**, 12 (2016).